Applied Catalysis B: Environmental 329 (2023) 122558

Contents lists available at ScienceDirect

Applied Catalysis B: Environmental

journal homepage: www.elsevier.com/locate/apcatb

Microenvironment modulation of cobalt single-atom catalysts for boosting both radical oxidation and electron-transfer process in Fenton-like system

Kexin Yin [a,1], Ruixian Wu [a,1], Yanan Shang [b,*], Dongdong Chen [a], Zelin Wu [c], Xinhao Wang [c], Baoyu Gao [a], Xing Xu [a,*]

[a] Shandong Key Laboratory of Water Pollution Control and Resource Reuse, School of Environmental Science and Engineering, Shandong University, Qingdao 266237, PR China
[b] College of Safety and Environmental Engineering, Shandong University of Science and Technology, Qingdao 266590, PR China
[c] State Key Laboratory of Hydraulics and Mountain River Engineering, College of Architecture and Environment, Sichuan University, Chengdu 610065, PR China

ARTICLE INFO

Keywords:
Cobalt
Single-atom catalysts
Peroxymonosulfate
Carbamazepine
Electron-transfer

ABSTRACT

Two coordination structures (Co-N_4 or Co-N_3) of cobalt single-atom catalysts (Co-SACs) were prepared by using the chitosan as starting precursor to evaluate the modulated coordination microenvironment of Co-SACs for organics degradation. The degradation performances for carbamazepine (CBZ) as well as the radical/nonradical pathways in Co-N_4/PMS and Co-N_3/PMS systems was evaluated. Results showed that more radicals could be produced by the Co-N_3 catalyst via stronger PMS adsorption as well as the subsequent peroxide bond cleavage of PMS. In addition, a lower energy gap between the CBZ and Co-N_3/PMS complex was endowed for the Co-N_3 coordination to boost stronger electron-transfer process for CBZ. As a result, both radical and electron-transfer process was boosted by the coordinated Co-N_3 sites than those of Co-N_4 coordination. This work provides a new insight on the versatile catalytic pathways with modulated coordination microenvironment of carbon-based SACs for high-efficiency PMS activation.

1. Introduction

Recently, the persulfate-mediated Fenton-like reactions using peroxydisulfate (PDS) or peroxymonosulfate (PMS) to generate highly active sulfate radical ($SO_4^{\bullet-}$) for the degradation of organics have been intensively investigated [1]. Homogeneous catalysis via various transition-metal (TM) ions (e.g., Fe^{2+}, Co^{2+}, Mn^{2+}, and Cu^{2+}) have showed high efficiency in the persulfate activation [1–4]. However, some disadvantages including the sluggish regeneration, difficult separation and sludge generation after homogeneous catalysis greatly limited the utilization of TM ions [4–6]. Heterogeneous catalysts using various metal nanoparticles (e.g., Fe_0, $CuFe_2O_4$, Co_3O_4, CuO, MnO_2, and Mn_2O_3) have been considered as an alternative to the homogeneous catalysis [7–12]. However, the metal nanoparticles with the inhomogeneity of active centers showed relatively lower catalytic activity as compared with their homogeneous counterparts, partially due to the restricted utilization efficiency of surface metal atoms as well as the reduced proton transfer for Fenton-like catalysis [13,14].

Recently, the metal nanoparticles have been downsized to the isolated single-atom metal sites with confined onto the specific supports, which have been defined as single-atom catalysts (SACs) [15,16]. The SACs have succeeded in bridging the gap of homogeneous and heterogeneous catalysis by inheriting the advantages of both homogeneous and heterogeneous catalysts. SACs have achieved maximized atomic utilization efficiency and exhibited high catalytic activity and selectivity in a variety of heterogeneous catalysis, including environmental catalysis such as persulfate-based Fenton-like systems [15]. Carbon-based SACs with nitrogen coordinated with the metal single atom (M-N bond) are mostly reported because of the abundant sources of carbon and nitrogen precursors [17]. As a result, a variety of carbon-based SACs with versatile M-N_x coordination have been prepared, which showed versatile catalytic pathways for organics degradation via PMS/PDS activation [17,18]. Shang et al. have reported that the coordination environment of SACs was critical to the catalytic behaviors and catalytic pathways [15,17]. This may be due to electronic metal-support interactions resulted from the multiple electronegativity of metal atoms that can regulate the local electronic properties or spin states of the single-atom metal sites in the SACs [19,20]. However, recent studies have reported some different

* Corresponding authors
E-mail addresses: shangyanan@sdust.edu.cn (Y. Shang), xuxing@sdu.edu.cn (X. Xu).
[1] They both are co-first authors

https://doi.org/10.1016/j.apcatb.2023.122558
Received 18 July 2022; Received in revised form 11 January 2023; Accepted 1 March 2023
Available online 2 March 2023

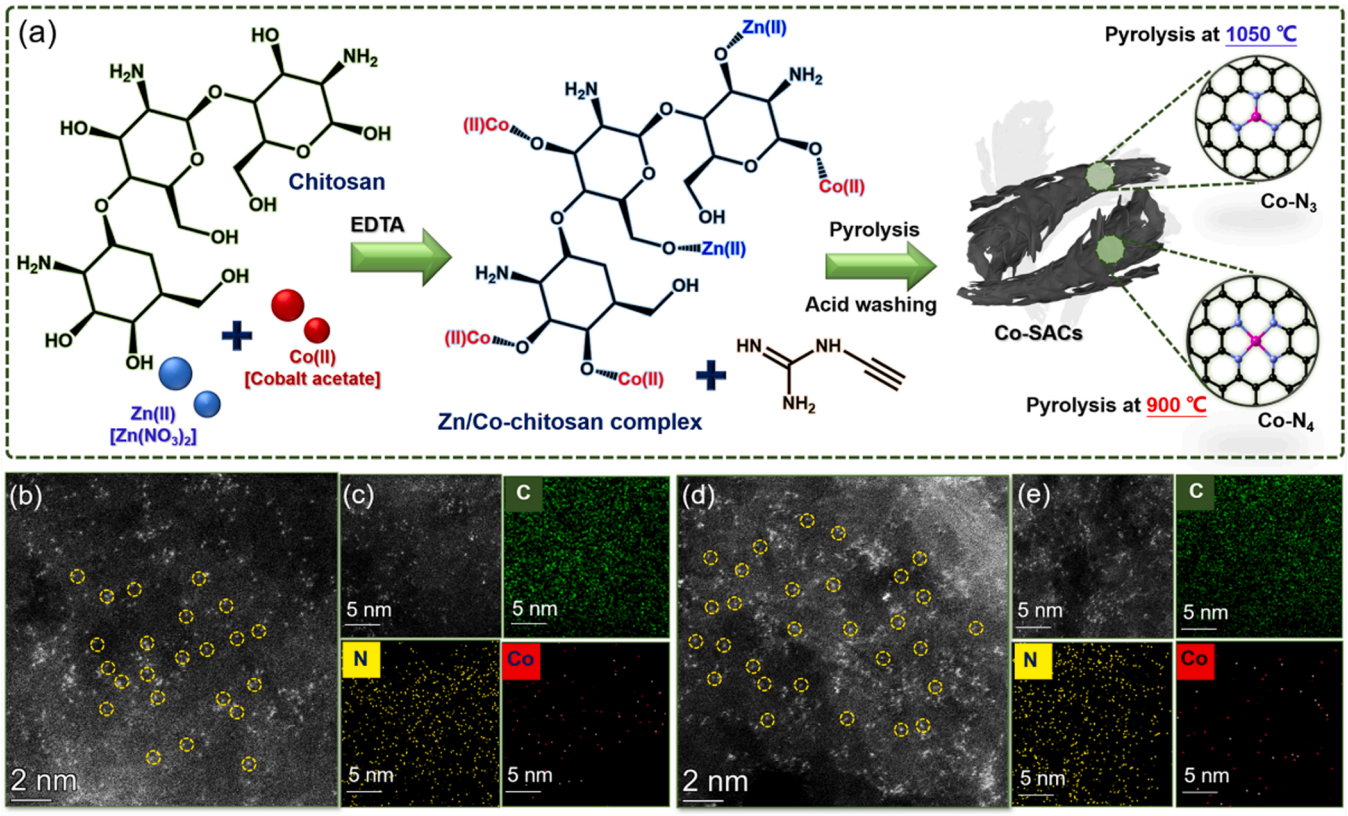

Fig. 1. (a) Fabricating scheme of Co-N_3 and Co-N_4 catalysts using chitosan as starting material; (b) HADDF-HRTEM of Co-N_3 catalyst; (c) HRTEM mappings of Co-N_3; (d) HADDF-HRTEM of Co-N_4; (e) HRTEM mappings of Co-N_4 catalyst.

catalytic mechanisms for the same pollutants via PMS/PDS activation even by the same coordination structures of M-N_x. For example, Chu et al. reported the radical-dominated degradation for the degradation of BPA in Co-N_4/PMS system [21], while various nonradical pathways (e.g., singlet oxygen, and electron-transfer) were also induced via PMS activation by the Co-N_4 site and acted as the major degradation pathways towards the BPA and other pollutants [22–24]. This might be due to the different carbon substances used for confining the M-N_x site that affected the electronic metal-support interactions in the carbon-based SACs [21–24]. Another important issue was that the M-N_x site was not always precisely coordinated but comprised of both M-N_{x-1}, M-N_x or M-N_{x+1} [15,25,26].

To solve the above issues, two coordination structures (Co-N_4 and Co-N_3) of Co-SACs were prepared by using the deacetylated chitosan as starting precursor via the modulation of pyrolysis temperature at 850 and 1000 °C, respectively. The coordination numbers can be controlled via varying the pyrolysis temperature to modulate the nitrogen release [27]. The degradation performances for carbamazepine (CBZ) as well as the radical/nonradical pathways in Co-N_4/PMS and Co-N_3/PMS systems was evaluated. Results showed that more radicals could be generated via stronger PMS adsorption as well as the subsequent peroxide bond cleavage of PMS by the Co-N_3 catalyst as compared with that of Co-N_4 catalyst. We also found that both Co-N_4 and Co-N_3 sites could modulate the microenvironment of carbon substance for promoting the electron-transfer process, while a lower energy gap between the CBZ and Co-N_3/PMS complex was endowed for the Co-N_3 coordination to boost stronger electron-transfer process for CBZ. As a result, both radical and electron-transfer process was boosted by the coordinated Co-N_3 than that of Co-N_4 coordination. This work provides a new insight into the versatile degradation pathways with modulated coordination microenvironments of carbon-based SACs for PMS activation.

2. Materials and methods

2.1. Chemicals

The deacetylated chitosan, 5,5-dimethyl-1-pyrroline N-oxide (DMPO), PMS, furfuryl alcohol (FFA), and tert-butyl alcohol (TBA), cobalt acetate, zinc nitrate, ethyl alcohol (EtOH), ethylene diamine tetraacetic acid (EDTA), dicyandiamide, and 2,2,6,6-Teramethyl-4-piperidinol (TEMP) were purchased from Sinopharm Chemical Reagent Co. Ltd. The organic pollutants, including carbamazepine (CBZ), bisphenol A (BPA), p-chlorophenol (CP), metronidazole (MNZ), p-nitrophenol (PNP), phenol (PE), were obtained from Aladdin Co. Ltd., China.

2.2. Preparation of chitosan-based Co-SACs

Two coordination structures (Co-N_4 or Co-N_3) of Co-SACs were prepared by using the deacetylated chitosan as starting precursor. The deacetylated chitosan (10 g), EDTA (3.0 g), cobalt nitrate (28 mmol), and $Zn(NO_3)_2{\cdot}6\,H_2O$ (28 mmol) was first ultrasonically dispersed in 500 mL of deionized water, and stirred for 60 min. The addition of EDTA could help to chelate more metal ions onto the chitosan framework. Subsequently, the Co/Zn-chitosan complex was rinsed with deionized water, dried for 12 h at 80 °C. It was mixed with 10 times weight of dicyandiamide and fully grinded. The mixed powder was pyrolyzed in a quartz tubular furnace at 550 ℃ for 1 h and 900 ℃ for another 1 h under N_2 atmosphere to obtained the Co-SAC with Co-N_4 coordination. The Co-SAC with Co-N_3 coordination was obtained by increasing the second-step pyrolysis temperature to 1050 ℃ to control the nitrogen release. Zn atoms help disperse the Co atoms in the carbon skeleton, which evaporated with temperature higher than 600 ℃ [28,29]. In addition, metal-free catalyst (N-C) was prepared by the same procedures without

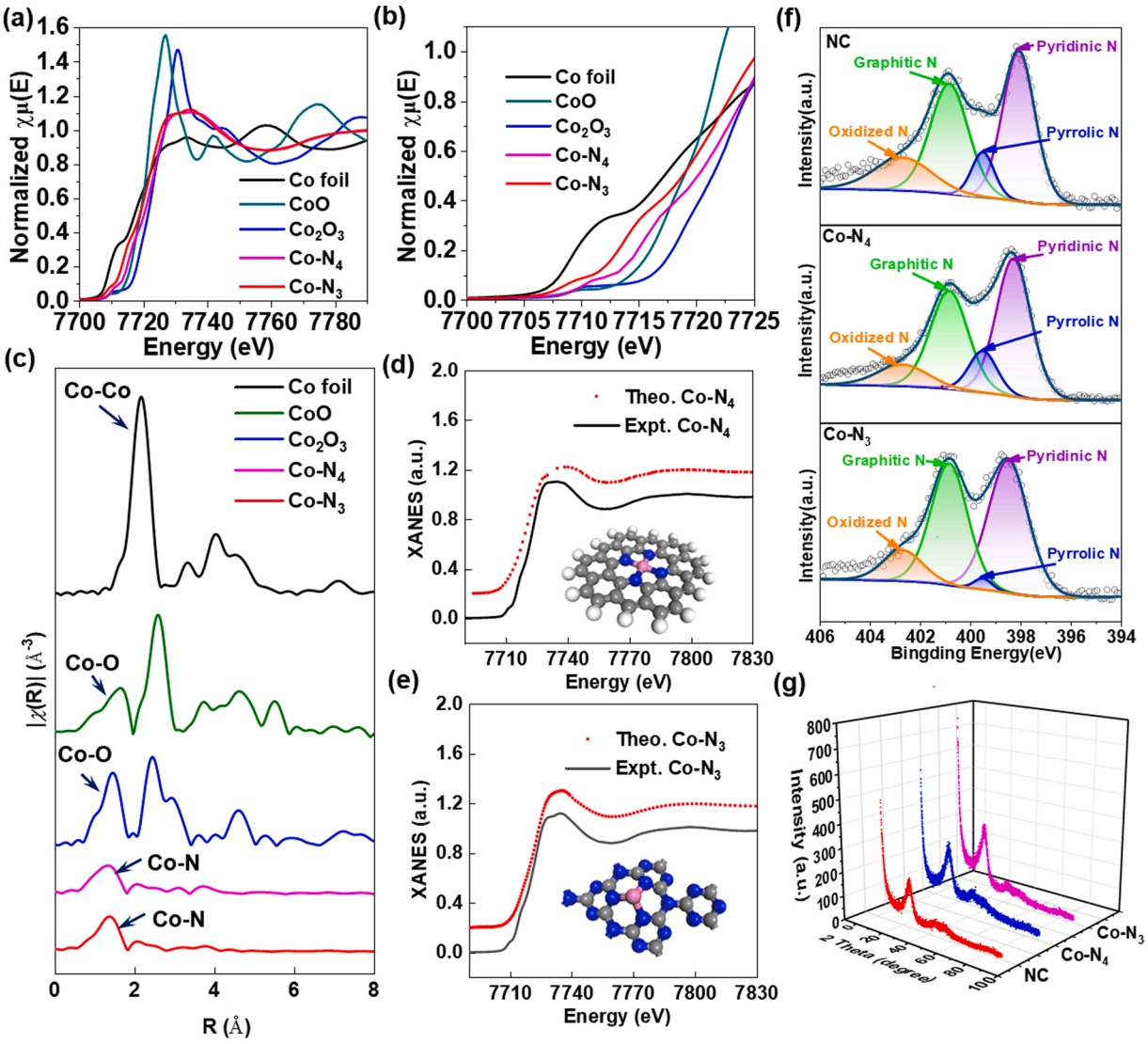

Fig. 2. (a) XANES of Co-N_3 and Co-N_4 catalysts at energy of 7690–7780 eV; (b) Energy at 7700–7725 eV; (c) FT-EXAFS of the two Co-SACs; (d) WT-EXAFS spectra of Co-N_3 and Co-N_4 catalysts; (d-e) Comparison between the experimental K-edge XANES spectra and the theoretical spectra of (d) Co-N_4 and (e) Co-N_3 catalysts (The gray, blue and pink balls refer to C, N, and Co atoms, respectively). (e) XPS N 1s spectra of N-C, Co-N_4 and Co-N_3 catalysts; (f) XRD patterns of N-C, Co-N_4 and Co-N_3 catalysts.

adding the metal salts.

2.3. Degradation of organics via PMS activation

The degradation of CBZ was performed by adding PMS (0.5 mM) and catalyst (0.1 g/L) into 50 mL CBZ solution (10 mg/L). The suspension (1 mL) was withdrawn at required time interval and filtered via a 0.22 μm film. The filtrate was mixed with 0.5 mL methanol, and then the residual concentration of CBZ were determined by a high-performance liquid chromatograph (HPLC, UltiMate 3000) with a C-18 column. Quenching experiment was conducted by adding different quenching agents including EtOH, TBA, and TEMP into the catalytic system to determine the corresponding reactive oxygen species (ROS) in both Co-N_3/PMS and Co-N_4/PMS systems. D_2O as solution was employed to replace the H_2O for determining the role of singlet oxygen ($^1O_2$). The stability of Co-N_3 operated under different PMS dosages (0.5 and 2.0 mM) was appraised by means of cycling experiments. During each run, the catalyst was separated through filtration followed by washing with deionized water and drying at 60 °C, which was then subjected to the next run of CBZ degradation.

Pristine carbon felt was first cut into small pieces of uniform size (1 cm^3), and 2.5 g of carbon felt fragments were weighed. The Co-N_3 (15 mg) was mixed with 120 μL of nafion in 3 mL N,N-dimethylformamide, and then the mixture was added to the carbon felt fragments in-drop. Subsequently, 5 mL of methanol and 20 mL of deionized water were dropped into the carbon felt until it was just soaked, and ultrasound for 1 min to make the dispersion of Co-N_3 more uniform. The fragments of loaded with Co-N_3 dried in an oven at 70 °C for 24 h. Finally, the carbon felt was packed in a column with a diameter of 1 cm and a length of 20 cm. The catalytic filter tests were then conducted by feeding the mixed CBZ and PMS solution from bottom to top for continuous operation. Other experimental procedures, including electrochemical measurements (voltammetry, and open circuit potential), electron paramagnetic resonance (EPR), residual PMS detection and density functional theory (DFT) calculation were given in Appendix S1-S7.

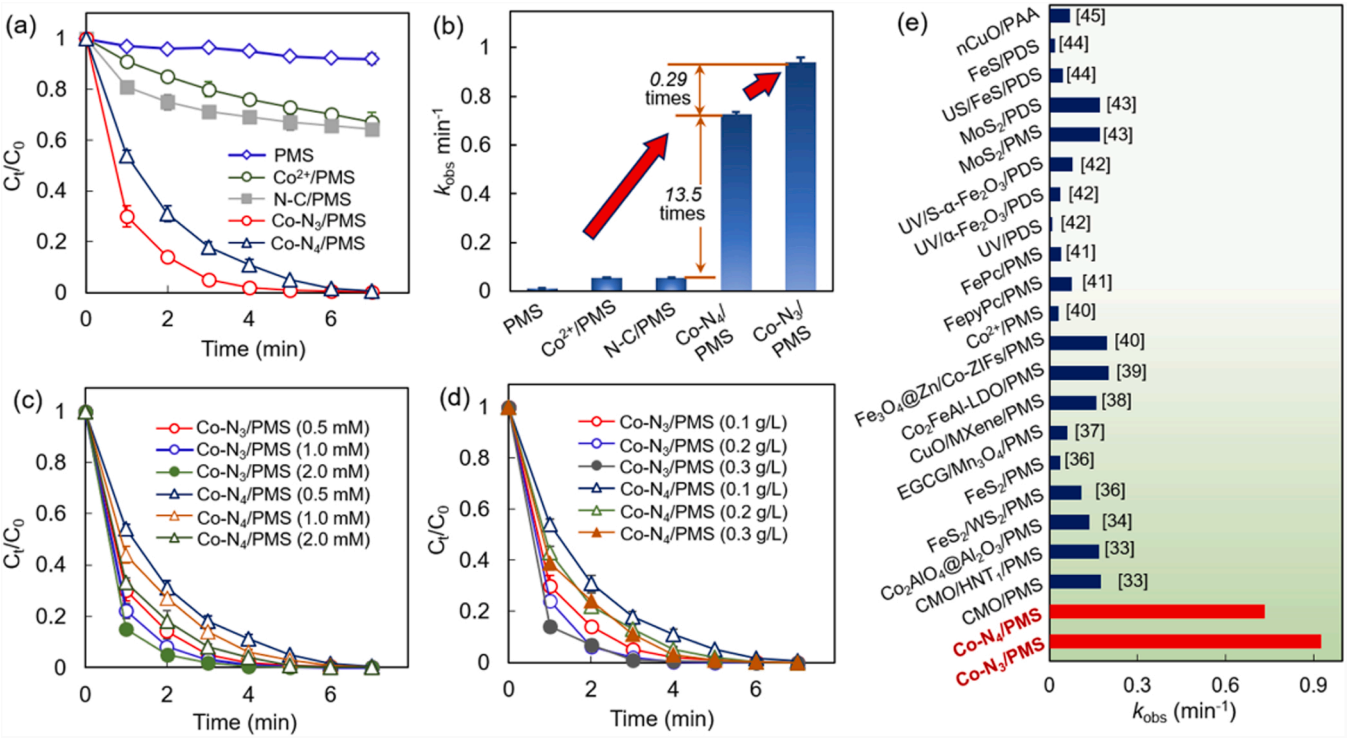

Fig. 3. (a) Degradation of CBZ in different catalytic systems; (b) The k_{obs} values of CBZ in different catalytic systems; (c) CBZ oxidation in Co-N_4/PMS and Co-N_3/PMS systems with different PMS dosages, (d) CBZ oxidation in Co-N_4/PMS and Co-N_3/PMS systems with different catalyst dosage; (e) Comparison of the k_{obs} of CBZ in different catalytic systems. (CBZ concentration: 10 mg/L; PMS dosage: 0.5 mM; catalyst dosage: 0.1 g/L).

3. Results and discussions

3.1. Characteristics of Co-N_3 and Co-N_4 catalysts

HADDF-HRTEM technique can visualize the atomically-dispersed metal sites in the supporting matrixes [28,30]. The HADDF-HRTEM images of Co-N_3 and Co-N_4 catalysts were given in Fig. 1b-e. Some isolated light spots can be observed in the chitosan-based carbon matrixes (Fig. 1b and d). EDS element mappings of the as-prepared catalysts showed that both nitrogen and cobalt species were well dispersed in the scale of 5–10 nm, and no cobalt species was aggregated to form the cobalt nanoparticles (Fig. 1c and e). These results indicated that the atomically-dispersed Co sites have been successfully anchored onto the carbon substances. XRD patterns of the Co-N_3 and Co-N_4 showed the similar peaks as compared with the N-C sample, and no specific peak of cobalt nanoparticles can be observed (Fig. S1), which further confirmed the formation of single Co atoms in the chitosan-based carbon matrixes. The Co amounts in both catalysts were detected, and the contents of Co were approximately 2.45–2.51 wt%.

The X-ray absorption spectroscopy (XAS) could provide the precise coordination environments (e.g., coordination numbers, coordination structures, and valence states) in as-prepared Co-SACs. The X-ray absorption near-edge structure (XANES) of two Co-SACs indicated that the absorption edge of atomically-dispersed Co-N_3 and Co-N_4 sites were located between the CoO and Co_2O_3 (Fig. 2a and b), unveiling a range of Co^{2+} and Co^{3+} of their valence states. A shift towards lower energy from Co-N_4 to Co-N_3 can be observed, reflecting the decreased oxidation state of Co [31]. The accurate coordination information of the two Co-SACs was verified by quantitative EXAFS fitting analysis (Figs. 2c and S2). The Fourier transform extended X-ray absorption fine structure (FT-EXAFS) of the two Co-SACs showcased a prominent peak at 1.45 Å (Fig. 2c), which was ascribed to the coordination of the single-atom Co with N atoms. After EXAFS fitting, the Co-N coordination numbers in the two Co-SACs were calculated to be 3.1 and 4.0, respectively (Table S2); this confirmed that the Co-N_3 and Co-N_4 configurations were the dominated coordination structures in the as-prepared Co-SACs [32,33]. We also calculated the XANES of both Co-N_3 and Co-N_4 models, and compared them with their experimental spectra (Fig. 2d and e). Results showed that the theoretically calculated spectra of Co-N_3, and Co-N_4 exhibited similar features to the experimental results. For example, the position and shape of the peak in experimental spectrum of Co-N_3 at about 7732 eV was quite similar to the theoretical Co-N_3 result. All these results further demonstrated well-defined Co-N_3 and Co-N_4 configurations in the two Co-SACs catalysts. N1s XPS spectra of the two Co-SACs and N-C catalysts showed a small shift (0.4 eV) of pyridinic N in both Co-N_3 and Co-N_4 catalysts as compared with that of N-C. No shifts of graphitic N, pyrrolic N, and nitric oxide can be observed [14,22,23]. As a result, the Co single-atom was coordinated with pyridine N to form the Co-N_3 or Co-N_4 configurations (Fig. 2f). XRD patterns of Co-N_3 and Co-N_4 catalysts showed the similar graphitic peak as compared with that of N-C catalyst, and no specific Co crystal peaks can be observed (Fig. 2g). These results further confirmed the absence of aggregated Co-NPs in both Co-N_3 and Co-N_4 catalysts [34].

3.2. Comparison of catalytic performances in Co-N_3/PMS and Co-N_4/PMS systems

Degradation of CBZ in different catalytic systems was shown in Figs. 3a and S3. Both Co-N_4/PMS and Co-N_3/PMS systems showed ultrafast oxidation activity with 100% of CBZ decomposition at 6 min. The lower N-coordinated Co-N_3 exhibited a higher activation activity towards PMS than that of the Co-N_4 coordinated catalyst, which showed 0.29-fold enhancement in the CBZ degradation (Fig. 3b). In contrast, only approximately 30–35% of CBZ was oxidized in Co^{2+}/PMS and N-C/PMS systems. The degradation rate (k_{obs}) of Co-N_4/PMS was ~13.5 times higher than those of Co^{2+}/PMS and N-C/PMS systems (Fig. 3b). CBZ degradation in Co-N_4/PMS and Co-N_3/PMS systems showed a steady increase in with the increasing PMS dosages (Figs. 3c, and S4a).

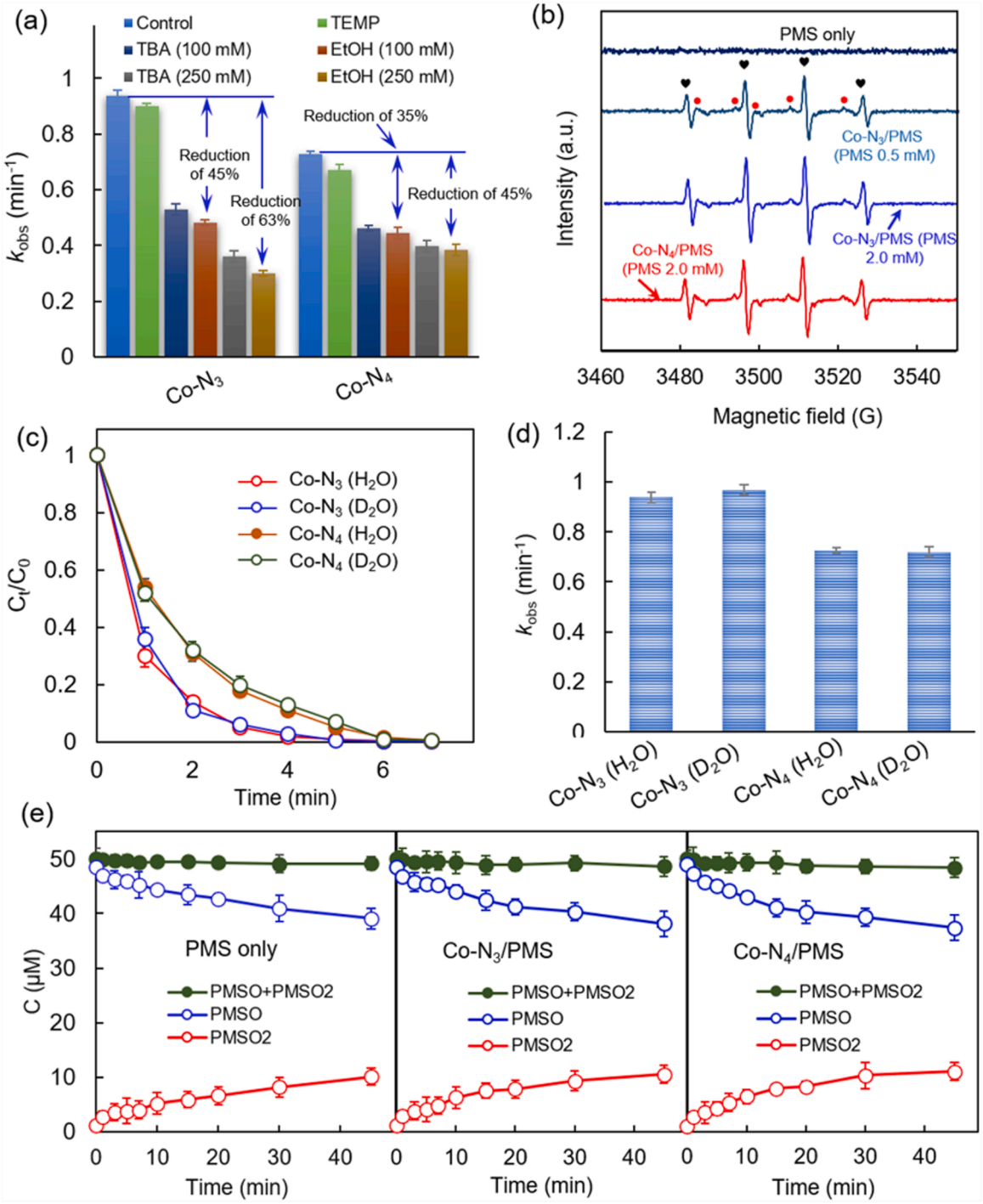

Fig. 4. (a) The k_{obs} values of CBZ oxidation in Co-N_3/PMS and Co-N_4/PMS systems by using different scavengers; (b) DMPO adducts in PMS only, Co-N_3/PMS (0.5 mM), Co-N_3/PMS (2.0 mM), and Co-N_4/PMS (2.0 mM) systems; (c) CBZ oxidation in Co-N_3/PMS and Co-N_4/PMS systems by replacement of H_2O with D_2O; (d) The k_{obs} of CBZ oxidation in H_2O and D_2O solutions; (e) PMSO and $PMSO_2$ concentrations at PMS of 0.5 mM in PMS alone, Co-N_3/PMS, and Co-N_4/PMS systems. (CBZ concentration: 10 mg/L; PMS dosage: 0.5 mM; catalyst dosage: 0.1 g/L).

Increasing the amounts of Co-SACs could also provide more single-atom Co active sites for CBZ degradation. However, the activity capacity was becoming saturated at catalyst dosage of 0.1 g/L (Figs. 3d, and S4b), and therefore, the k_{obs} was only increased by approximately 20% with catalyst dosage increasing from 0.1 to 0.3 g/L. Comparison of the k_{obs} of CBZ degradation with other reported catalytic systems were given in Fig. 3e and Table S3. Results indicated that the degradation performances of CBZ in Co-N_4/PMS and Co-N_3/PMS systems exhibited almost one or two orders of magnitude higher than those of various metal nanoparticles/PMS(PDS) systems and homogeneous Fenton-like systems [35–47]. This result showcased the exceptional excellent Fenton-like catalytic activities of the single-atom Co active sites for organics degradation.

3.3. *Comparison of catalytic mechanisms in Co-N_3/PMS and Co-N_4/PMS systems*

Quenching experiments in Co-N_3/PMS and Co-N_4/PMS systems by

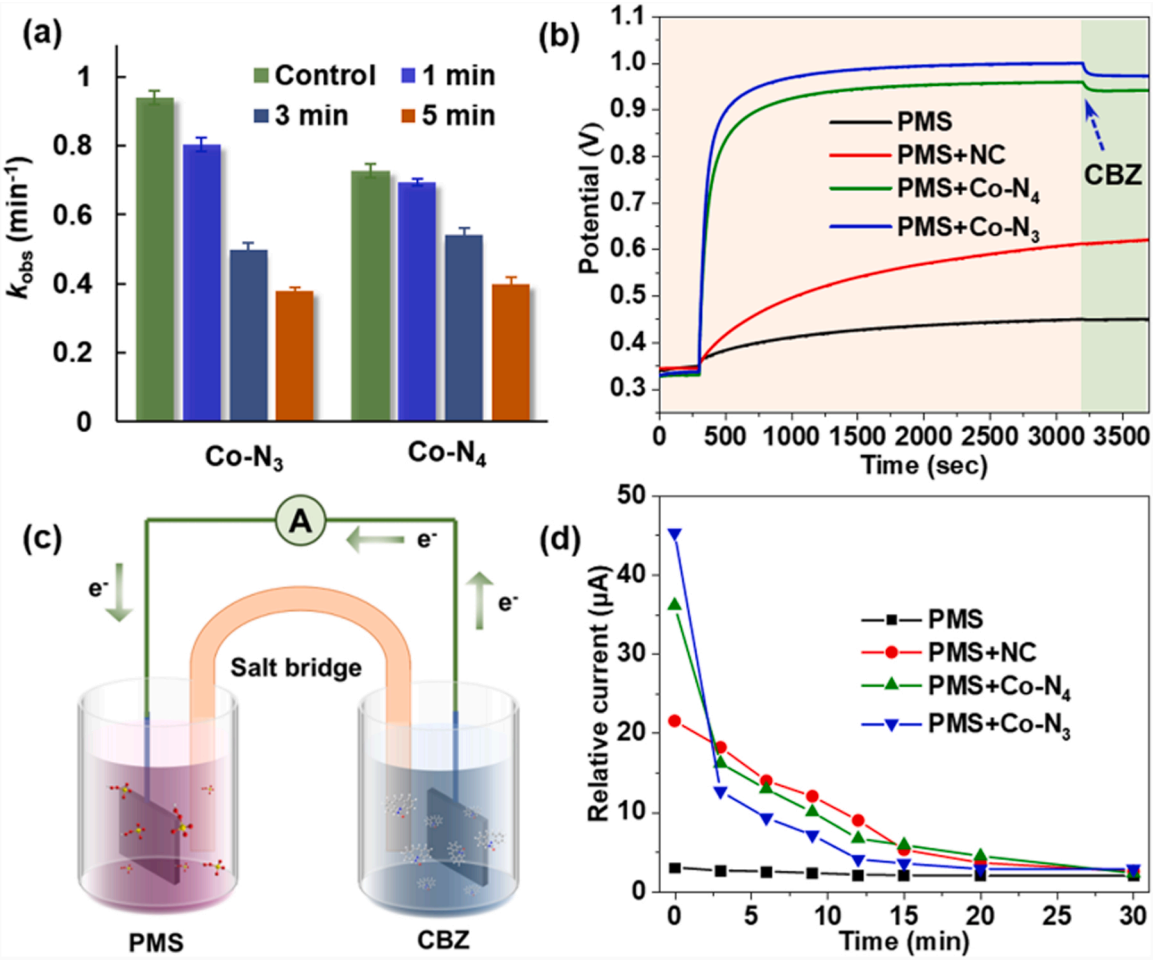

Fig. 5. (a) The k_{obs} of CBZ oxidation in Co-N_3/PMS and Co-N_4/PMS systems with premixing catalyst and PMS (CBZ concentration: 10 mg/L; PMS dosage: 0.5 mM; catalyst dosage: 0.1 g/L); (b) Open-potential in Co-N_3/PMS and Co-N_4/PMS systems; (c) A scheme of galvanic oxidation system; (d) Current generation in GOS coating with different catalysts (Co-N_3, Co-N_4, and N-C).

using different scavengers were shown in Figs. 4a and S5. Although both radical and singlet oxygen ($^1O_2$) scavengers only retard the complete CBZ degradation from 5 min to 10–15 min in the both Co-N_3/PMS and Co-N_4/PMS systems (Fig. S6), a certain difference in the quenching results for the targeted Co-SACs can be observed. The EtOH and TBA using as radical scavengers showed more quenching effect in the Co-N_3/PMS system than that in Co-N_4/PMS system (Fig. 4a). For example, the k_{obs} of CBZ degradation was reduced more than 60% in the Co-N_3/PMS system by adding 250 mM of TBA, which was relatively higher than that (45%) in the Co-N_4/PMS system. This result indicated that more radicals ($HO^•$ and $SO_4^{•-}$) can be produced in the Co-N_3/PMS system. DMPO adducts in Co-N_3/PMS system showed that the signals of $HO^•$ and $SO_4^{•-}$ both increased with the increasing catalytic time (Fig. S7). What's more, the signals of $HO^•$ and $SO_4^{•-}$ in Co-N_3/PMS system was higher than those in Co-N_4/PMS system (Fig. 4b), which further confirmed the stronger catalytic activity of Co-N_3 for PMS activation to generate the radicals ($HO^•$ and $SO_4^{•-}$). TEMP as $^1O_2$ probe showed only a very small effect on the CBZ degradation and the role of $^1O_2$ can be further determined by using D_2O as solvent since the lifetime of $^1O_2$ can be prolonged in D_2O (Figs. 4a and S5). Results shown in Fig. 4c and d indicated that the CBZ degradation was almost constant by replacement of H_2O with D_2O, which showcased the negligible role of $^1O_2$ in the CBZ degradation. In addition, the PMSO consumption and $PMSO_2$ production in the Co-SAC/PMS systems were also evaluated by compared with the PMS alone system, since PMSO could be oxidized to either hydroxylated MPSO/biphenyl compounds via radical ($SO_4^{•-}$ and $HO^•$) based oxidation or to generate $PMSO_2$ by the high-valent metal-oxo species [48,49]. As shown in Fig. 4e, approximately 20% of PMSO was consumed at PMS (0.5 mM) alone system, while the consumptions of PMSO in both Co-N_3/PMS, and Co-N_4/PMS systems were also similar to that in PMS alone system. Since the PMS can also react with the PMSO to form $PMSO_2$ but with slower oxidating rate, these results indicated that both Co-N_3 and Co-N_4 catalysts did not participate in the consumption of PMSO. As a result, high-valent cobalt-oxo oxidation was not involved in the Co-N_3/PMS and Co-N_4/PMS systems.

Since the radicals were generated via the reaction between the PMS and catalysts, premixing the catalysts (Co-N_3, and Co-N_4) and PMS in the catalytic system before the addition of CBZ was conducted to identify the role of radicals for CBZ degradation, and the results were shown in Figs. 5a and S8. Increasing premixing times from 1 min to 5 min showed a steady decrease in the k_{obs} of CBZ, and more reduction in k_{obs} of CBZ can be observed in Co-N_3/PMS system. This result further confirmed the generation of more radicals for CBZ degradation in Co-N_3/PMS system. However, complete degradation of CBZ was only retarded from 5 min to 10 min in both Co-N_3/PMS and Co-N_4/PMS systems (Fig. S8), which indicated that although radicals contributed to the CBZ degradation in both catalytic systems, the degradation of CBZ was mostly controlled by other nonradical pathways.

Open-circuit potentials can be useful for determining the electron-transfer pathway in the catalytic system. Extraordinary different potential change was observed in varied catalysts/PMS/CBZ systems (Fig. 5b). The oxidation potentials of different catalysts/PMS systems

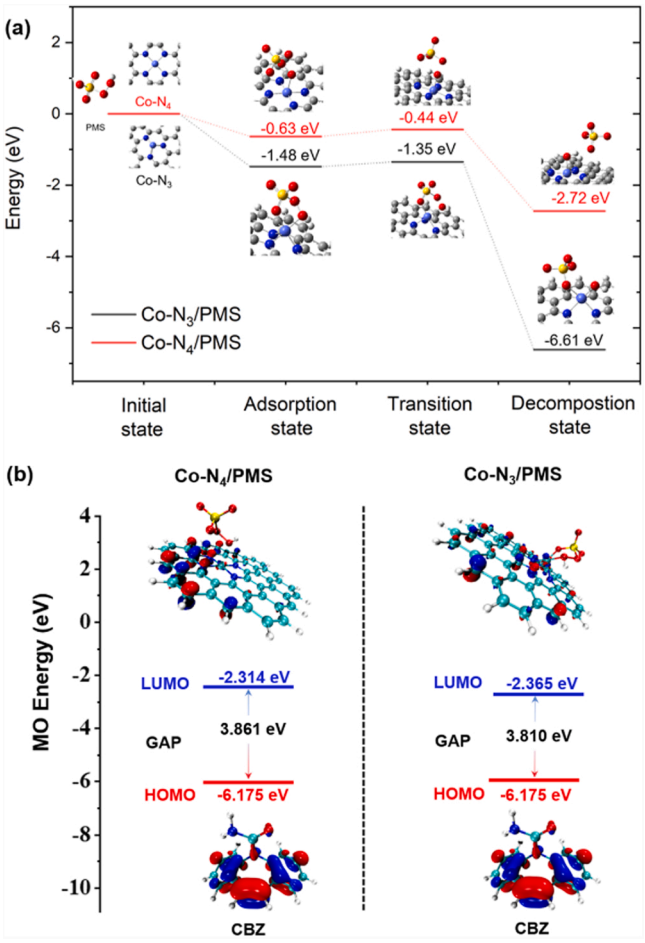

Fig. 6. (a) Energy barriers of radical pathways in Co-N_4/PMS and Co-N_3/PMS systems; (b) Gaps of LUMO of Co-N_3/PMS or Co-N_4/PMS and HOMO of CBZ.

were triggered from approximately 0.33 V to 0.95 V in Co-N_4/PMS and 1.0 V in Co-N_3/PMS. This result indicated that the Co-N_3 could form stronger metastable intermediate with PMS (Co-N_3/PMS*) than that (Co-N_4/PMS*) of Co-N_4 [50]. In contrast, the degradation potential was evaluated to 0.6 V by the metal-free N-C. In addition, the addition of CBZ showed a reduction in the potential of Co-N_3/PMS* and Co-N_4/-PMS* , while a very weak fluctuation of potential was observed in the N-C/PMS/CBZ system. These results indicated that strong electron-transfer process for CBZ occurred in the Co-N_3/PMS and Co-N_4/PMS systems. In addition, a galvanic oxidation system (GOS) was carried out to further evaluate the electron-transfer between the CBZ and varied catalysts/PMS* intermediates since the electrons can transfer from the pollutant to catalysts/PMS* intermediates along with electron channel if the electron-transfer process occurred in the catalytic systems [51]. CBZ and PMS were added into two independent cells that were connected by an agar salt bridge and an ampere meter (Fig. 5c). The graphite electrode in the cells were loaded with different catalysts (Co-N_3, Co-N_4, and N-C). GOS coating with Co-N_3 showed a high instantaneous current of 45 μA (Fig. 5d), and it was followed by the Co-N_4 (36 μA) and N-C (22 μA). Such results confirmed that Co-N_3 could trigger more electron-transfer than the Co-N_4 and N-C. In addition, more CBZ could be oxidized by the Co-N_3 catalyst in the GOS (Fig. S9), which indicated that more electron-transfer process could be induced via PMS activation by the Co-N_3 for CBZ degradation.

3.4. DFT analysis

DFT analysis was further carried out to unveil the catalytic pathways of the two coordination structures for CBZ degradation. The adsorption configurations of PMS/Co-SACs via combination between Co and various oxygen atom in PMS was investigated by DFT calculation (Fig. S10). For Co-N_4/PMS, three configurations showed close adsorption energy (E_{ads}=−0.63 to 0.60 eV). However, the three configurations of Co-N_3/PMS showed larger adsorption energy (E_{ads}=−1.20∼−1.48 eV), which suggested PMS was more to be easily combined with Co-N_3 configuration. It was worth noting that Co atom in Co-N_3 bulged out the carbon plane, while the configurations of Co-N_4 is a pure plane structure. The bulging out Co in Co-N_3 made the PMS prefer to be combined via two oxygen atoms due to less steric-hinderance effect, which showed larger adsorption energy and more thermodynamic stability. The stronger E_{ads} of Co-N_3 with PMS would facilitate the dissociation of O-O bond in PMS via elongating the l_{O-O} of PMS. The energy barriers of radical pathways in Co-N_4/PMS and Co-N_3/PMS systems were also calculated and the results were given in Fig. 6a. The Gibbs free energies for the formation of radicals ($SO_4^{\bullet-}$, and •OH) were much lower than the reactant, exhibiting the thermodynamically favorable process for $SO_4^{\bullet-}$ and •OH generation in the Co-SACs/PMS systems [5]. The favorable single-atom sites for the formation of $SO_4^{\bullet-}$ and •OH with lowest Gibbs free energy was based on the Co-N_3 configuration rather than the Co-N_4 configuration [5]. As a result, the generation of more radicals could be induced by the Co-N_3 coordination, which was consistent with EPR and quenching tests. LUMO of different complexes (Co-N_3/PMS or Co-N_4/PMS) and HOMO of CBZ were given in Fig. 6b. The HOMO (−6.175 eV) of CBZ was more negative as compared with the LUMO (−2.314 ∼ −2.365 eV) of Co-N_3/PMS or Co-N_4/PMS complexes, implying the electrons migration from the HOMO of CBZ to the LUMO of catalysts/PMS complexes [52,53]. In addition, the gap (3.810 eV) between HOMO of CBZ and LUMO of Co-N_3/PMS complex was smaller than that (3.861 eV) between HOMO of CBZ and LUMO of Co-N_4/PMS complex. This result indicated that the electrons can be more easily extracted from CBZ to the PMS via Co-N_3 sites as the bridges, and therefore, facilitating the electron-transfer process of CBZ in Co-N_3/PMS system.

3.5. Degradation performance in Co-N_3/PMS system

Adsorption and degradation of CBZ in Co-N_3/PMS system under different pH conditions were given in Figs. S11 and 7a. Adsorption of CBZ was almost constant (∼20%) under pH range of 3.0–10.0. The CBZ degradation showed a steady descend trend as the pH increased from 3.0 to 10.0 with k_{obs} in the range of 0.872–0.989 min^{-1}. The k_{obs} of CBZ adsorption under different pH conditions accounted for a very small proportion to the CBZ removal as compared with those of CBZ degradation (Fig. 7b). The Co ions under different pH conditions indicated that approximately 0.06 mg/L of Co^{2+} ions were released from the Co-N_3 catalyst at acidic condition (pH 3.0), and it was decreased to 0.010–0.015 mg/L under neutral and alkaline environments (Fig. S12). In addition, approximately 2–3% of CBZ could be oxidized via homogeneous catalysis of leached Co^{2+} (Fig. 7c). CBZ degradation in Co-N_3/PMS system with the background of different anions (Cl^-, NO_3^-, HCO_3^-, PO_4^{3-}) and HA showed that almost 100% of CBZ degradation still could be achieved with the interference of these substances (Fig. S13). However, a noticeable reduction in the k_{obs} was inevitable which might due to their quenching effect on the reactive oxygen species (Fig. S14). Stability test under different PMS dosages (0.5, and 2.0 mM) was also conducted and the results were given in Fig. 7e. Results showed that adding more PMS could improve the degradation of CBZ in the first cycle, however the increase of PMS dosage would substantially reduce the stability of the Co-N_3 (Fig. 7f). The degradation of CBZ in Co-N_3/PMS system was less depended on the PMS dosage, while the addition of more PMS would be adsorbed or consumed onto the surface of Co-N_3 catalyst (Fig. S15). Although the adsorbed PMS could be activated to generate the radicals for CBZ degradation, saturated PMS adsorption but without fully PMS decomposition would also result in the active site poisoning

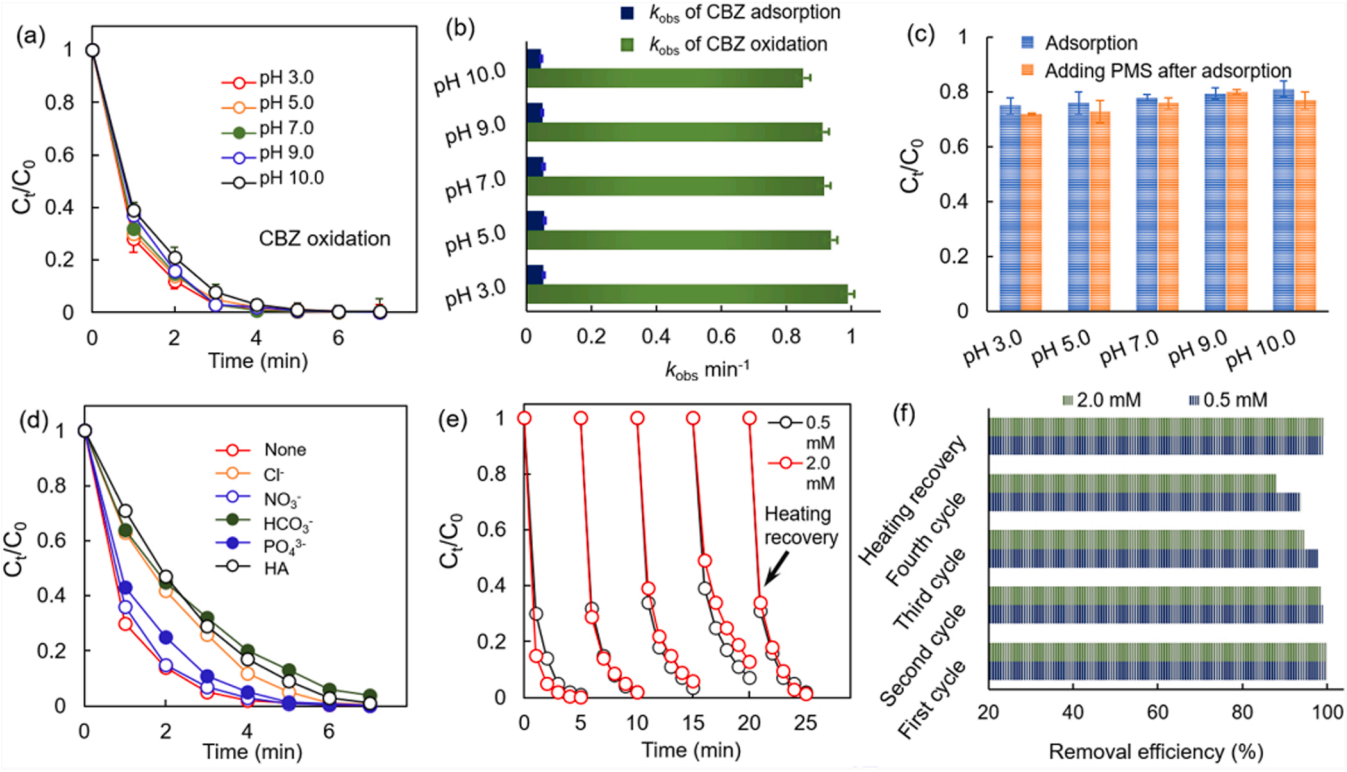

Fig. 7. (a) The degradation of CBZ in Co-N_3/PMS system under different pH conditions; (b) k_{obs} values of CBZ adsorption and degradation in Co-N_3/PMS system; (c) CBZ degradation by the leached Co ion in Co-N_3/PMS system under different pH conditions; (d) CBZ degradation in Co-N_3/PMS system with the background of different anions; (e) Stability test of Co-N_3 under different PMS dosages; (f) Removal efficiency of CBZ after different cycles. (CBZ concentration: 10 mg/L; PMS dosage: 0.5 mM; catalyst dosage: 0.1 g/L).

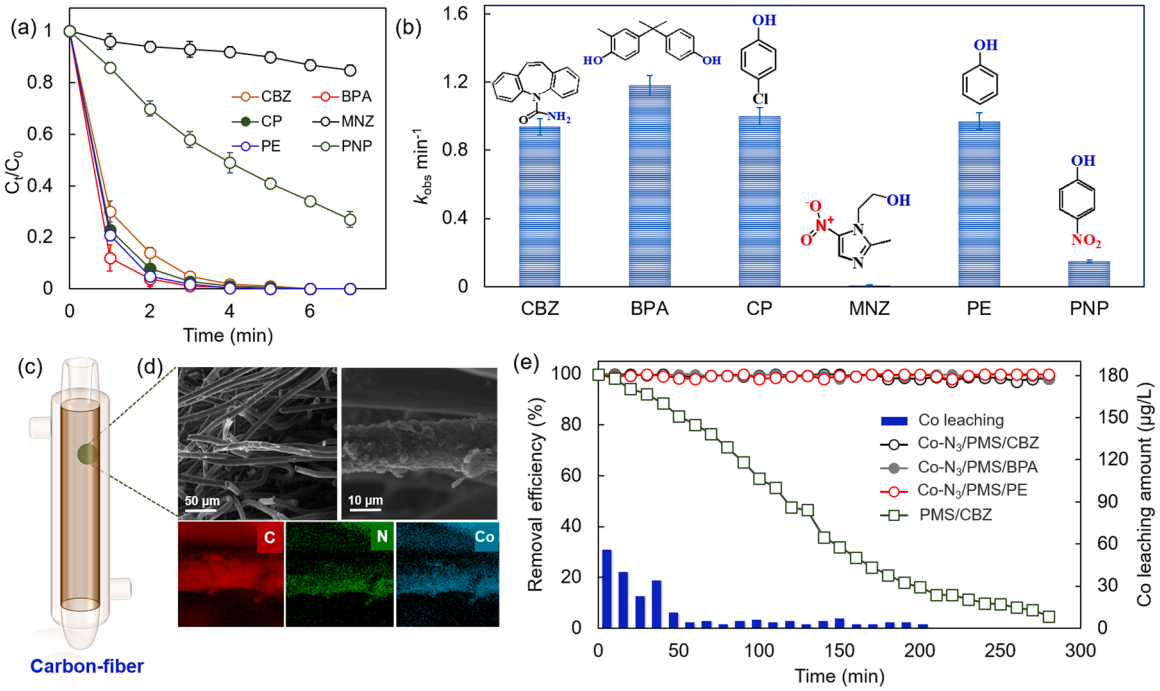

Fig. 8. (a) Degradation of different organics in Co-N_3/PMS system (organics concentration: 10 mg/L; PMS dosage: 0.5 mM; catalyst dosage: 0.1 g/L); (b) The k_{obs} values of different organics in Co-N_3/PMS system; (c) Scheme of catalytic carbon-fiber filter; (d) SEM of the Co-N_3 coated carbon-fiber; (e) Degradation of different pollutants in the Co-N_3 coated catalytic filter (Co-N_3 dosage: 15 mg).

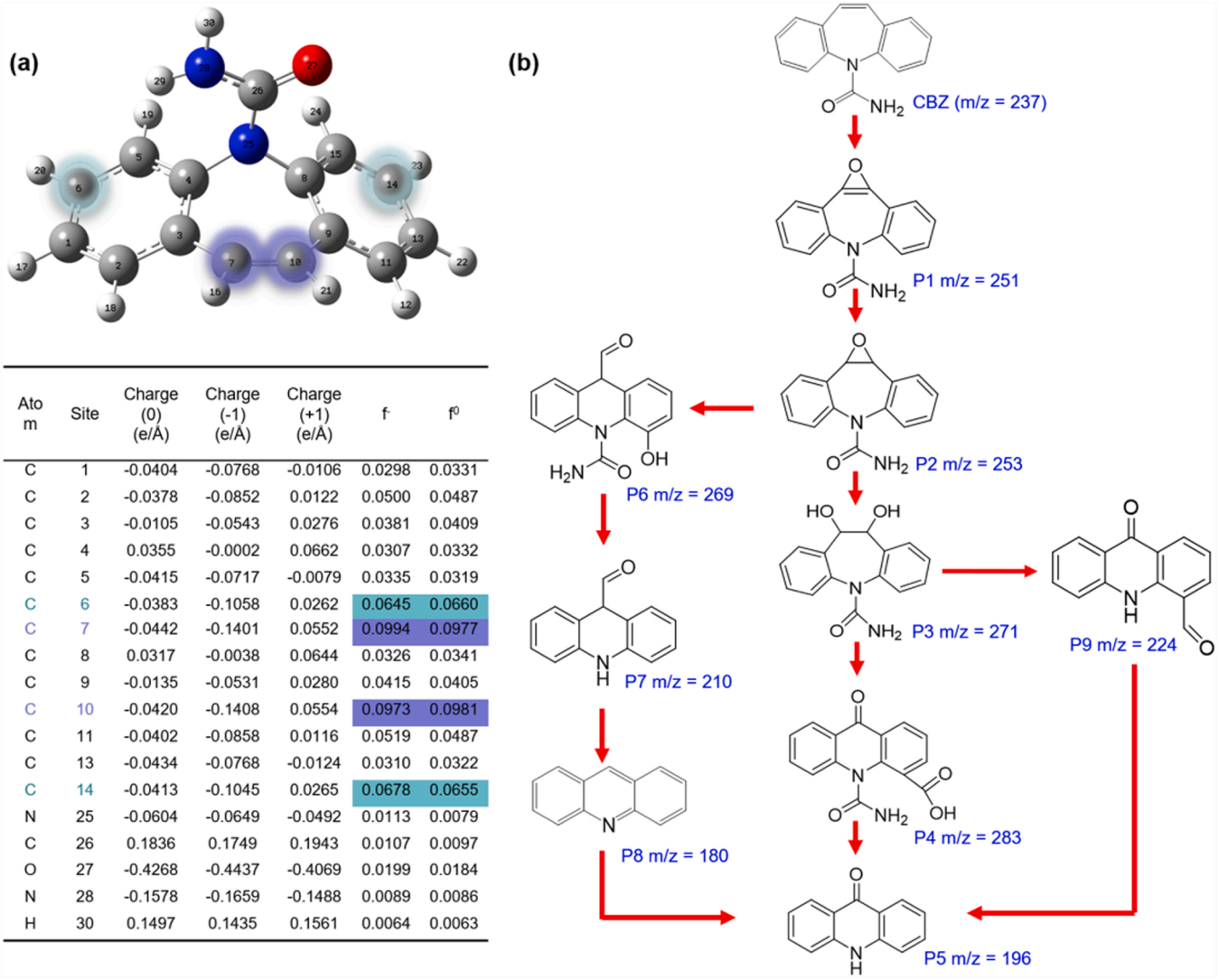

Atom	Site	Charge (0) (e/Å)	Charge (-1) (e/Å)	Charge (+1) (e/Å)	f⁻	f⁰
C	1	-0.0404	-0.0768	-0.0106	0.0298	0.0331
C	2	-0.0378	-0.0852	0.0122	0.0500	0.0487
C	3	-0.0105	-0.0543	0.0276	0.0381	0.0409
C	4	0.0355	-0.0002	0.0662	0.0307	0.0332
C	5	-0.0415	-0.0717	-0.0079	0.0335	0.0319
C	6	-0.0383	-0.1058	0.0262	0.0645	0.0660
C	7	-0.0442	-0.1401	0.0552	0.0994	0.0977
C	8	0.0317	-0.0038	0.0644	0.0326	0.0341
C	9	-0.0135	-0.0531	0.0280	0.0415	0.0405
C	10	-0.0420	-0.1408	0.0554	0.0973	0.0981
C	11	-0.0402	-0.0858	0.0116	0.0519	0.0487
C	13	-0.0434	-0.0768	-0.0124	0.0310	0.0322
C	14	-0.0413	-0.1045	0.0265	0.0678	0.0655
N	25	-0.0604	-0.0649	-0.0492	0.0113	0.0079
C	26	0.1836	0.1749	0.1943	0.0107	0.0097
O	27	-0.4268	-0.4437	-0.4069	0.0199	0.0184
N	28	-0.1578	-0.1659	-0.1488	0.0089	0.0086
H	30	0.1497	0.1435	0.1561	0.0064	0.0063

Fig. 9. (a) Fukui values of all atoms in the CBZ molecule; (b) Possible transformation pathways of CBZ in the Co-N_3/PMS system.

[22], which would impede the subsequent cycle for CBZ degradation. HADDF-HRTEM of Co-N_3 catalyst as well as XANES of Co-N_3 catalyst before and after PMS activation were shown in Figs. S16 and S17. Results showed that no Co single atoms are agglomerated into Co clusters and its valence state was also not changed. In addition, heating recovery (350 °C) could greatly improve the catalytic activity of the spent Co-N_3 catalyst, which might be due to the decomposition of PMS as well as the CBZ intermediates attached on the Co-N_3 catalyst.

Degradation of different pollutants in the Co-N_3/PMS system exhibited that the Co-N_3 could effectively oxidize the broad-spectrum pollutants via PMS activation, but also exhibited a certain extent of degradation selectivity (Fig. 8a and b). The k_{obs} values of pollutants (e.g., CBZ, PE, BPA, and CP) with electron-rich group (e.g., hydroxy group) in the Co-N_3/PMS system were approximately in the range of 0.9–1.2 min^{-1}. In contrast, degradation of pollutants (e.g., SMX, and PNP) with electron-deficient group (e.g., nitro group) was inert in the Co-N_3/PMS system. The carbon felt was packed with 30 mg of Co-N_3 catalyst to form the catalytic filter and the mixture of pollutants and PMS was feed to the catalytic filter from bottom to top (Fig. 8c). SEM image of the Co-N_3 packed catalytic filter showed that the filter was composed of the high-density carbon fibers (Fig. 8d). The EDS mappings indicated that the Co-N_3 catalysts were well dispersed on the surface of the carbon fibers, thus forming large numbers of single-atom cobalt sites for PMS activation. Catalytic results showed that the CBZ, BPA and PE could be completely oxidized in the catalytic filter for more than 250 min. In contrast, the carbon felt without coating Co-N_3 showed poor degradation performance of CBZ. These results indicated the high-efficiency of Co-N_3 coated catalytic filter for continuous operation. The Co leaching during the long-time operation was also detected (Fig. 8e). Approximately 50 μg/L of Co was leached at first 10 min, and it was gradually decreased to lower than 5 μg/L with the further operation, which indicated the stability of the Co-N_3 in the catalytic filter.

3.6. Degradation intermediates of CBZ in Co-N_3/PMS system

The intermediates of CBZ in the Co-N_3/PMS system were detected by ultra-performance liquid chromatography combined with quadrupole time-of-flight mass spectrometry (UPLCQ-TOF-MS/MS), and their structural formulas are derived by the accurate mass and fragment ions (Fig. S18). The active sites on the CBZ molecule were first instructed by the Fukui index. As shown in Fig. 9a, the C7 and C10 of the CBZ molecule marked with purple circles showed the highest f^- values, which were most vulnerable to the electrophilic species. The transformation pathways of CBZ were proposed according to its intermediates, as shown in Fig. 9b. The degradation of CBZ first occurred on the C7 and C10 due to their highest f^- values and formed the epoxy group in the CBZ molecule (P1), and it was followed by the hydrogeneration (P2) on the epoxidized CBZ and further epoxide cleavage to

accept hydroxyl group (P3). The P3 can be transformed into the P4 due to the bond cleavage of C7-C10, and the bond of N25-C26 can be attacked to form the P5. Besides, the synchronous bond cleavages of C7-C10 and N25-C26 in P3 occurred, which was accompanied with the formylation to form the P9, and can be further transformed into the P5. Due to the high f^- values of C7 and C10, the bond of C7-C10 can also be easily attacked in the epoxidized intermediate (P2) after hydrogeneration to the form the acylated intermediate (P6). It can be further transformed into the P7 and P8 after the deamidation and diacylation.

4. Conclusions

Two coordination structures (Co-N_4 and Co-N_3) of Co-SACs were prepared by using the chitosan as starting precursor via the modulation of pyrolysis temperature at 850 and 1000 °C, respectively. The coordination numbers can be controlled via varying the pyrolysis temperature to modulate the nitrogen release. The degradation performances for carbamazepine (CBZ) as well as the radical/nonradical pathways in Co-N_4/PMS and Co-N_3/PMS systems was evaluated. Results showed that more radicals could be generated via stronger PMS adsorption as well as the subsequent peroxide bond cleavage of PMS by the Co-N_3 catalyst as compared with that of Co-N_4 catalyst. In addition, both single-atom Co sites could modulate the microenvironment of carbon substance for promoting the electron-transfer process, while a lower energy gap between the CBZ and Co-N_3/PMS complex was endowed for the Co-N_3 coordination to boost stronger electron-transfer process for CBZ. As a result, both more radical and electron-transfer process was boosted by the Co-N_3 than that of Co-N_4 coordination. This work provides a new insight into the versatile catalytic pathways with modulated coordination microenvironment of carbon-based SACs for PMS activation.

CRediT authorship contribution statement

Kexin Yin: Methodology, Formal analysis, Investigation, Writing – original draft, Visualization. **Ruixian Wu:** Visualization. **Yanan Shang:** XASF analysis, DFT calculation. **Dongdong Chen:** Methodology. **Zelin Wu:** Formal analysis, Investigation. **Xinhao Wang:** Visualization. **Baoyu Gao**: Methodology. **Xing Xu:** Resources, Writing – review & editing, Supervision.

Declaration of Competing Interest

The authors declare that they have no known competing financial interests or personal relationships that could have appeared to influence the work reported in this paper.

Data availability

Data will be made available on request.

Acknowledgments

The research work was supported by National Natural Science Foundation of China (52170086) and Natural Science Foundation of Shandong Province (ZR2021ME013). The authors also want to thank Conghua Qi from Shiyanjia Lab (www.shiyanjia.com). In addition, X.D. acknowledges the financial support from Australian Research Council under DECRA scheme (DE210100253).

Appendix A. Supplementary material

Supplementary data associated with this article can be found in the online version at doi:10.1016/j.apcatb.2023.122558.

References

[1] G.P. Anipsitakis, D.D. Dionysiou, Radical generation by the interaction of transition metals with common oxidants, Environ. Sci. Technol. 38 (2004) 3705–3712, https://doi.org/10.1021/es035121o.
[2] C. Jiang, S. Garg, T.D. Waite, Hydroquinone-mediated redox cycling of iron and concomitant oxidation of hydroquinone in oxic waters under acidic conditions: comparison with iron–natural organic matter interactions, Environ. Sci. Technol. 49 (2015) 14076–14084, https://doi.org/10.1021/acs.est.5b03189.
[3] Y.-Y. Ahn, H. Bae, H.-I. Kim, S.-H. Kim, J.-H. Kim, S.-G. Lee, J. Lee, Surface-loaded metal nanoparticles for peroxymonosulfate activation: efficiency and mechanism reconnaissance, Appl. Catal. B Environ. 241 (2019) 561–569, https://doi.org/10.1016/j.apcatb.2018.09.056.
[4] J. Pan, B. Gao, P. Duan, K. Guo, X. Xu, Q. Yue, Recycling exhausted magnetic biochar with adsorbed Cu2+ as a cost-effective permonosulfate activator for norfloxacin degradation: Cu contribution and mechanism, J. Hazard. Mater. 413 (2021), 125413, https://doi.org/10.1016/j.jhazmat.2021.125413.
[5] B. Zhang, X. Li, K. Akiyama, P. Bingham, S. Kubuki, Elucidating the mechanistic origin of a spin state-dependent FeNx−C catalyst toward organic contaminant oxidation via peroxymonosulfate activation, Environ. Sci. Technol. 56 (2022) 1321–1330, https://doi.org/10.1021/acs.est.1c05980.
[6] J. Wang, H. B, M. Yang, R. Liu, C. Hu, H. Liu, J. Qu, Anaerobically-digested sludge disintegration by transition metal ions-activated peroxymonosulfate (PMS): comparison between Co2+, Cu2+, Fe2+ and Mn2, Sci. Total Environ. 713 (2020), 136530, https://doi.org/10.1016/j.scitotenv.2020.136530.
[7] E. Saputra, S. Muhammad, H. Sun, H.-M. Ang, M.O. Tadé, S. Wang, Shape-controlled activation of peroxymonosulfate by single crystal α-Mn2O3 for catalytic phenol degradation in aqueous solution, Appl. Catal. B Environ. 154–155 (2014) 246–251, https://doi.org/10.1016/j.apcatb.2014.02.026.
[8] H. Liang, H. Sun, A. Patel, P. Shukla, Z.H. Zhu, S. Wang, Excellent performance of mesoporous Co3O4/MnO2 nanoparticles in heterogeneous activation of peroxymonosulfate for phenol degradation in aqueous solutions, Appl. Catal. B Environ. 127 (2012) 330–335, https://doi.org/10.1016/j.apcatb.2012.09.001.
[9] T. Zhang, Y. Chen, Y. Wang, J. Le Roux, Y. Yang, J.-P. Croué, Efficient peroxydisulfate activation process not relying on sulfate radical generation for water pollutant degradation, Environ. Sci. Technol. 48 (2014) 5868–5875.
[10] Y. Ma, H. Wang, X. Lv, D. Xiong, H. Xie, Z. Zhang, Three-dimensional ordered mesoporous Co3O4/peroxymonosulfate triggered nanoconfined heterogeneous catalysis for rapid removal of ranitidine in aqueous solution, Chem. Eng. J. 443 (2022), 136495, https://doi.org/10.1016/j.cej.2022.136495.
[11] L. Zhao, J. Zhang, Z. Zhang, T. Wei, J. Wang, J. Ma, Y. Ren, H. Zhang, Co3O4 crystal plane regulation to efficiently activate peroxymonosulfate in water: the role of oxygen vacancies, J. Colloid Interface Sci. 623 (2022) 520–531, https://doi.org/10.1016/j.jcis.2022.05.045.
[12] Y. Su, M. Lu, R. Su, W. Zhou, X. Xu, Q. Li, A 3D MIL-101@rGO composite as catalyst for efficient conversion of straw cellulose into valuable organic acid, Chin. Chem. Let. 33 (2022) 2573–2578, https://doi.org/10.1016/j.cclet.2021.08.078.
[13] W.-D. Oh, Z. Dong, T.-T. Lim, Generation of sulfate radical through heterogeneous catalysis for organic contaminants removal: current development, challenges and prospects, Appl. Catal. B Environ. 194 (2016) 169–201, https://doi.org/10.1016/j.apcatb.2016.04.003.
[14] Y. Zhu, R. Zhu, Y. Xi, J. Zhu, G. Zhu, H. He, Strategies for enhancing the heterogeneous Fenton catalytic reactivity: a review, Appl. Catal. B Environ. 255 (2019), 117739, https://doi.org/10.1016/j.apcatb.2019.05.041.
[15] Y. Shang, X. Xu, B. Gao, S. Wang, X. Duan, Single-atom catalysis in advanced oxidation processes for environmental remediation, Chem. Soc. Rev. 50 (2021) 5281–5322, https://doi.org/10.1039/D0CS01032D.
[16] B. Qiao, A. Wang, X. Yang, L.F. Allard, Z. Jiang, Y. Cui, J. Liu, J. Li, T. Zhang, Single-atom catalysis of CO oxidation using Pt1/FeOx, Nat. Chem. 3 (2011) 634–641, https://doi.org/10.1038/nchem.1095.
[17] Y. Shang, X. Duan, S. Wang, Q. Yue, B. Gao, X. Xu, Carbon-based single atom catalyst: Synthesis, characterization, DFT calculations, Chin. Chem. Let. 33 (2022) 663–673, https://doi.org/10.1016/j.cclet.2021.07.050.
[18] J. Pan, B. Gao, P. Duan, K. Guo, M. Akram, X. Xu, Q. Yue, Y. Gao, Improving peroxymonosulfate activation by copper ion-saturated adsorbent-based single atom catalysts for the degradation of organic contaminants: electron-transfer mechanism and the key role of Cu single atoms, J. Mater. Chem. A 9 (2021) 11604–11613, https://doi.org/10.1039/D1TA02237G.
[19] W. Liu, L. Zhang, X. Liu, X. Liu, X. Yang, S. Miao, W. Wang, A. Wang, T. Zhang, Discriminating catalytically active FeNx species of atomically dispersed Fe–N–C catalyst for selective oxidation of the C–H bond, J. Am. Chem. Soc. 139 (2017) 10790–10798, https://doi.org/10.1021/jacs.7b05130.
[20] J. Miao, Y. Zhu, J. Lang, J. Zhang, S. Cheng, B. Zhou, L. Zhang, P.J.J. Alvarez, M. Long, Spin-state-dependent peroxymonosulfate activation of single-atom M–N moieties via a radical-free pathway, ACS Catal. 11 (2021) 9569–9577, https://doi.org/10.1021/acscatal.1c02031.
[21] C. Chu, J. Yang, X. Zhou, D. Huang, H. Qi, S. Weon, J. Li, M. Elimelech, A. Wang, J.-H. Kim, Cobalt single atoms on tetrapyridomacrocyclic support for efficient peroxymonosulfate activation, Environ. Sci. Technol. 55 (2021) 1242–1250, https://doi.org/10.1021/acs.est.0c06086.
[22] X. Li, X. Huang, S. Xi, S. Miao, J. Ding, W. Cai, S. Liu, X. Yang, H. Yang, J. Gao, J. Wang, Y. Huang, T. Zhang, B. Liu, Single cobalt atoms anchored on porous N-doped graphene with dual reaction sites for efficient Fenton-like catalysis, J. Am. Chem. Soc. 140 (2018) 12469–12475, https://doi.org/10.1021/jacs.8b05992.
[23] H. Xu, N. Jiang, D. Wang, L. Wang, Y. Song, Z. Chen, J. Ma, T. Zhang, Improving PMS oxidation of organic pollutants by single cobalt atom catalyst through hybrid

radical and non-radical pathways, Appl. Catal. B Environ. 263 (2020), 118350, https://doi.org/10.1016/j.apcatb.2019.118350.
[24] X. Peng, J. Wu, Z. Zhao, X. Wang, H. Dai, Y. Wei, G. Xu, F. Hu, Activation of peroxymonosulfate by single atom Co-N-C catalysts for high-efficient removal of chloroquine phosphate via non-radical pathways: electron-transfer mechanism, Chem. Eng. J. 429 (2022), 132245, https://doi.org/10.1016/j.cej.2021.132245.
[25] Y. Qi, J. Li, Y. Zhang, Q. Cao, Y. Si, Z. Wu, M. Akram, X. Xu, Novel lignin-based single atom catalysts as peroxymonosulfate activator for pollutants degradation: Role of single cobalt and electron transfer pathway, Appl. Catal. B Environ. 286 (2021), 119910, https://doi.org/10.1016/j.apcatb.2021.119910.
[26] C. Zhu, Y. Nie, S. Zhao, Z. Fan, F. Liu, A. Li, Constructing surface micro-electric fields on hollow single-atom cobalt catalyst for ultrafast and anti-interference advanced oxidation, Appl. Catal. B Environ. 305 (2022), 121057, https://doi.org/10.1016/j.apcatb.2021.121057.
[27] X. Wang, Z. Chen, X. Zhao, T. Yao, W. Chen, R. You, C. Zhao, G. Wu, J. Wang, W. Huang, J. Yang, X. Hong, S. Wei, Y. Wu, Y. Li, Regulation of coordination number over single Co sites: triggering the efficient electroreduction of CO_2, Angew. Chem. Int. Ed. 57 (2018) 1944–1948, https://doi.org/10.1002/ange.201712451.
[28] H. Fei, J. Dong, D. Chen, T. Hu, X. Duan, I. Shakir, Y. Huang, X. Duan, Single atom electrocatalysts supported on graphene or graphene-like carbons, Chem. Soc. Rev. 48 (2019) 5207–5241, https://doi.org/10.1039/C9CS00422J.
[29] Y.-S. Wei, M. Zhang, R. Zou, Q. Xu, Metal–organic framework-based catalysts with single metal sites, Chem. Rev. 120 (2020) 12089–12174, https://doi.org/10.1021/acs.chemrev.9b00757.
[30] A.J. Han, B.Q. Wang, A. Kumar, Y.J. Qin, J. Jin, X.H. Wang, C. Yang, B. Dong, Y. Jia, J.F. Liu, X.M. Sun, Recent advances for MOF-derived carbon-supported single-atom catalysts, Small Methods 3 (2019) 1800471, https://doi.org/10.1002/smtd.201800471.
[31] X. Wang, Z. Chen, X. Zhao, T. Yao, W. Chen, R. You, C. Zhao, G. Wu, J. Wang, W. Huang, J. Yang, X. Hong, S. Wei, Y. Wu, Y. Li, Regulation of coordination number over single Co sites: triggering the efficient electroreduction of CO_2, Angew. Chem. Int. Ed. 57 (2018) 1944–1948, https://doi.org/10.1002/ange.201712451.
[32] A. Zitolo, V. Goellner, V. Armel, M.T. Sougrati, T. Mineva, L. Stievano, E. Fonda, F. Jaouen, Identification of catalytic sites for oxygen reduction in iron- and nitrogen-doped graphene materials, Nat. Mater. 14 (2015) 937–942, https://doi.org/10.1038/nmat4367.
[33] L. Zhao, Y. Zhang, L.-B. Huang, X.-Z. Liu, Q.-H. Zhang, C. He, Z.-Y. Wu, L.-J. Zhang, J. Wu, W. Yang, L. Gu, J.-S. Hu, L.-J. Wan, Cascade anchoring strategy for general mass production of high-loading single-atomic metal-nitrogen catalysts, Nat. Commum. 10 (2019) 1278, https://doi.org/10.1038/s41467-019-09290-y.
[34] M.A. Oturan, J.-J. Aaron, Advanced oxidation processes in water/wastewater treatment: principles and applications. a review, Crit. Rev. Environ. Sci. Technol. 44 (2014) 2577–2641, https://doi.org/10.1080/10643389.2013.829765.
[35] X. Yang, G. Wei, P. Wu, P. Liu, X. Liang, W. Chu, Novel halloysite nanotube-based ultrafine CoMn2O4 catalyst for efficient degradation of pharmaceuticals through peroxymonosulfate activation, Appl. Surf. Sci. 588 (2022), 152899, https://doi.org/10.1016/j.apsusc.2022.152899.
[36] M.-P. Zhu, J.-C.E. Yang, D. Delai Sun, B. Yuan, M.-L. Fu, Deciphering the simultaneous removal of carbamazepine and metronidazole by monolithic Co_2AlO_4@Al_2O_3 activated peroxymonosulfate, Chem. Eng. J. 436 (2022), 135201, https://doi.org/10.1016/j.cej.2022.135201.
[37] H. Song, R. Du, Y. Wang, D. Zu, R. Zhou, Y. Cai, F. Wang, Z. Li, Y. Shen, C. Li, Anchoring single atom cobalt on two-dimensional MXene for activation of peroxymonosulfate, Appl. Catal. B Environ. 286 (2021), 119898, https://doi.org/10.1016/j.apcatb.2021.119898.
[38] G. Gou, S. Kang, H. Zhao, C. Liu, N. Li, B. Lai, J. Li, Efficient peroxymonosulfate activation through a simple physical mixture of FeS2 and WS2 for carbamazepine degradation, Sep. Purif. Technol. 290 (2022), 120828, https://doi.org/10.1016/j.seppur.2022.120828.
[39] L. Zhu, Z. Shi, L. Deng, J. Chen, H. Zhang, Fabrication of Epigallocatechin-3-gallate (EGCG) functionalized Mn3O4 for enhanced degradation of carbamazepine with peroxymonosulfate activation, Process Saf. Environ. Prot. 158 (2022) 42–54, https://doi.org/10.1016/j.psep.2021.11.033.
[40] P. Yang, S. Li, L. Xiaofu, A. Xiaojing, D. Liu, W. Huang, Singlet oxygen-dominated activation of peroxymonosulfate by CuO/MXene nanocomposites for efficient decontamination of carbamazepine under high salinity conditions: performance and singlet oxygen evolution mechanism, Sep. Purif. Technol. 285 (2022), 120288, https://doi.org/10.1016/j.seppur.2021.120288.
[41] Q.-T. Sun, B.-D. Xu, J. Yang, T.-T. Qian, H. Jiang, Layered oxides supported Co-Fe bimetal catalyst for carbamazepine degradation via the catalytic activation of peroxymonosulfate, Chem. Eng. J. 400 (2020), 125899, https://doi.org/10.1016/j.cej.2020.125899.
[42] Z. Wu, Y. Wang, Z. Xiong, Z. Ao, S. Pu, G. Yao, B. Lai, Core-shell magnetic Fe3O4@Zn/Co-ZIFs to activate peroxymonosulfate for highly efficient degradation of carbamazepine, Appl. Catal. B Environ. 277 (2020), 119136, https://doi.org/10.1016/j.apcatb.2020.119136.
[43] J. Li, T. Xu, J. Gao, Z. Wang, G. Wang, W. Chen, W. Lu, Efficient peroxymonosulfate activation by N-rich pyridyl-iron phthalocyanine derivative for the elimination of pharmaceutical contaminants under solar irradiation, Chemosphere 299 (2022), 134464, https://doi.org/10.1016/j.chemosphere.2022.134464.
[44] J. Deng, C. Ye, A. Cai, L. Huai, S. Zhou, F. Dong, X. Li, X. Ma, S-doping α-Fe2O3 induced efficient electron-hole separation for enhanced persulfate activation toward carbamazepine oxidation: experimental and DFT study, Chem. Eng. J. 420 (2021), 129863, https://doi.org/10.1016/j.cej.2021.129863.
[45] H. Zhou, L. Lai, Y. Wan, Y. He, G. Yao, B. Lai, Molybdenum disulfide (MoS2): a versatile activator of both peroxymonosulfate and persulfate for the degradation of carbamazepine, Chem. Eng. J. 384 (2020), 123264, https://doi.org/10.1016/j.cej.2019.123264.
[46] W. Xiang, H. Chen, Z. Zhong, C. Zhang, X. Lu, M. Huang, T. Zhou, P. Yu, B. Zhang, Efficient degradation of carbamazepine in a neutral sonochemical FeS/persulfate system based on the enhanced heterogeneous-homogeneous sulfur-iron cycle, Sep. Purif. Technol. 282 (2022), 120041, https://doi.org/10.1016/j.seppur.2021.120041.
[47] L. Zhang, J. Chen, Y. Zhang, Y. Xu, T. Zheng, X. Zhou, Highly efficient activation of peracetic acid by nano-CuO for carbamazepine degradation in wastewater: the significant role of H2O2 and evidence of acetylperoxy radical contribution, Water Res. 216 (2022), 118322, https://doi.org/10.1016/j.watres.2022.118322.
[48] H. Li, Z. Zhao, J. Qian, B. Pan, Are free radicals the primary reactive species in Co (II)-mediated activation of peroxymonosulfate? New evidence for the role of the Co (II)-peroxymonosulfate complex, Environ. Sci. Technol. 55 (2021) 6397–6406, https://doi.org/10.1021/acs.est.1c02015.
[49] Y. Zong, X. Guan, J. Xu, Y. Feng, Y. Mao, L. Xu, H. Chu, D. Wu, Unraveling the overlooked involvement of high-valent cobalt-oxo species generated from the Cobalt(II)-activated peroxymonosulfate process, Environ. Sci. Technol. 54 (2020) 16231–16239, https://doi.org/10.1021/acs.est.0c06808.
[50] L. Peng, X. Duan, Y. Shang, B. Gao, X. Xu, Engineered carbon supported single iron atom sites and iron clusters from Fe-rich enteromorpha for Fenton-like reactions via nonradical pathways, Appl. Catal. B Environ. 287 (2021), 119963, https://doi.org/10.1016/j.apcatb.2021.119963.
[51] M. Luo, H. Zhang, P. Zhou, Z. Xiong, B. Huang, J. Peng, R. Liu, W. Liu, B. Lai, Efficient activation of ferrate(VI) by colloid manganese dioxide: comprehensive elucidation of the surface-promoted mechanism, Water Res. 215 (2022), 118243, https://doi.org/10.1016/j.watres.2022.118243.
[52] F. Chen, L.-L. Liu, J.-H. Wu, X.-H. Rui, J.-J. Chen, Y. Yu, Single-atom iron anchored tubular g-C3N4 catalysts for ultrafast Fenton-like reaction: roles of high-valency iron-oxo species and organic radicals, Adv. Mater. 34 (2022) 2202891, https://doi.org/10.1002/adma.202202891.
[53] M. Yang, Z. Hou, X. Zhang, B. Gao, Y. Li, Y. Shang, Q. Yue, X. Duan, X. Xu, Unveiling the origins of selective oxidation in single-atom catalysis via Co–N4–C intensified radical and nonradical pathways, Environ. Sci. Technol. 56 (2022) 11635–11645, https://doi.org/10.1021/acs.est.2c01261.